Journal of Power Sources 238 (2013) 478–484

Contents lists available at SciVerse ScienceDirect

Journal of Power Sources

journal homepage: www.elsevier.com/locate/jpowsour

In situ X-ray diffraction and electrochemical impedance spectroscopy of a nanoporous Li_2FeSiO_4/C cathode during the initial charge/discharge cycle of a Li-ion battery

Haitao Zhou, Mari-Ann Einarsrud, Fride Vullum-Bruer*

Department of Materials Science and Engineering, Norwegian University of Science and Technology, 7491 Trondheim, Norway

HIGHLIGHTS

- An *in situ* XRD cell was fabricated with conductive Kapton film as X-ray window.
- EIS was collected at varying states of charge for nanoporous Li_2FeSiO_4/C cathode.
- Coexistence of a $P2_1/n$ phase and a $Pmn2_1$ phase was observed during the first cycle.
- The XRD data showed that the $Pmn2_1$ phase dominated in the fully discharge state.
- An inductance loop observed in the EIS data confirms the phase transformation.

ARTICLE INFO

Article history:
Received 26 November 2012
Received in revised form
20 February 2013
Accepted 9 March 2013
Available online 19 April 2013

Keywords:
In situ XRD
Li-ion battery
Cathode
Li_2FeSiO_4/C
Nanostructuring

ABSTRACT

Understanding of the structural evolution of the cathode during the charge/discharge processes is crucial to describe the Li insertion/de-insertion mechanisms in a Li-ion battery. An *in situ* XRD cell has been specially fabricated to study a nanostructured electrode using a standard laboratory diffractometer. This cell was used to investigate phase transformations of a nanoporous Li_2FeSiO_4/C cathode in the initial charge/discharge cycle by *in situ* XRD as well as analyzing the full Li-ion battery by electrochemical impedance spectroscopy (EIS). The battery was operated in chronocoulometric mode for the *in situ* XRD and galvanostatic intermittent titration technique (GITT) mode for the EIS. Coexistence of two different polymorphs, $P2_1/n$ and $Pmn2_1$ of Li_2FeSiO_4, was observed in the *in situ* XRD patterns. The amount of $P2_1/n$ phase, which was the only phase present before cycling, decreased while the amount of $Pmn2_1$ phase increased during the first cycle. In the fully discharged state the $Pmn2_1$ phase appeared as the main phase. An inductive loop was observed in the impedance spectra which is believed to arise from the formation of a concentration cell ($Li|P2_1/n||Pmn2_1|Li$) from which current flows in opposition to the Li being intercalated/de-intercalated into and out of the $Li_{2-x}FeSiO_4$ electrode.

1. Introduction

The Li-ion battery is currently the battery technology with the highest energy density, volumetric as well as gravimetric. Since the cathode materials play an important role in the determination of energy density, safety and life cycle of Li-ion batteries, research and development of cathode materials is important for the further improvement of these batteries. Especially, the study of the structural evolution of the cathode during the charge/discharge process is crucial to understand the Li insertion/de-insertion mechanisms and to optimize these materials so as to achieve high performance and cyclability. *In situ* X-ray diffraction (XRD) is widely used to study the correlation between the electrode material's structural and electrochemical behavior [1]. This technique allows for observations of the structural changes of the material while inside a closed *in situ* XRD electrochemical cell, which eliminates the risk of contamination and changes occurring due to chemical reactions that might occur if the cell is disassembled prior to the analysis. Beryllium (Be) foil has been widely used as X-ray window on the cathode side of the *in situ* XRD cell operating in synchrotron source facilities [2–4]. However, the Be window oxidizes and becomes porous at a high operating voltage, and an attenuation of the signal occurs due to the path length varying with the diffraction angle, consequently

* Corresponding author. Present address: Department of Material Science and Engineering, Alfred Getzv. 2, 7491 Trondheim, Norway. Tel.: +47 735 93976; fax: +47 735 50203.
E-mail addresses: vullum@nt.ntnu.no, vullum@material.ntnu.no (F. Vullum-Bruer).

0378-7753/$ – see front matter © 2013 Elsevier B.V. All rights reserved.
http://dx.doi.org/10.1016/j.jpowsour.2013.03.193

resulting in a poor signal to noise ratio in the collected powder patterns. Hence the *in situ* X-ray cell with Be window is not an ideal design for operating in standard laboratory diffractometers. Especially, for certain types of cathode materials which contain nanoparticles, nanopores, secondary phases, and a carbon-coating, using a Be window will result in poor quality of the XRD patterns. To compensate for the shortcomings of the Be window an X-ray penetrable polymer film can be used as the seal between the cathode and the ambient air. For this purpose electrically conductive Kapton (a polyimide) is a particularly good choice which has been used as XRD window by Meulenkamp et al. [5] because it is chemically inert (except in strongly alkaline solutions), shows no sharp XRD peaks, and is stable at temperatures up to about 325 °C [6].

Another powerful method that can be used to investigate structural changes of the electrode material during cycling is electrochemical impedance spectroscopy (EIS). It is important to note that an electrochemical impedance spectrum contains information about the entire electrochemical cell and not only the cathode as is the case with XRD. However, one important feature of the impedance spectrum which can be used to indicate structural changes is an inductive loop in the low frequency region of the Nyquist plot. The inductive loop is defined as the property of an electric circuit that causes an electromotive force to be generated in it as a result of a change in the current flowing through the circuit [7]. Hong et al. [8] proposed that the volume change in the phase transformation between $LiFe_{0.9}Mg_{0.1}PO_4$ and $Li_{0.1}Fe_{0.9}Mg_{0.1}PO_4$ leads to elastic–plastic deformation and induces a potential hysteresis and an inductive loop when the applied energy is higher than the opposing elastic–plastic accommodation energy. Gnanaraj et al. [9] also observed the inductive loop in the impedance spectra of the graphite electrode during initial cycling, which was attributed to the formation of a $(Li_{1-x}C_6)/C_6$ concentration cell from which current flows in opposition to the Li being intercalated into the graphite. This kind of two-phase concentration-cell-induced inductive loops were also found in Nyquist plots obtained in other initial cycling studies where layered $LiCoO_2$ [10] and spinel $LiMn_2O_4$ [11] were used as cathodes in lithium ion batteries.

Recently, a Li_2FeSiO_4/C composite has been considered a promising candidate as cathode material for Li-ion batteries [12]. However, the structure of Li_2FeSiO_4 undergoes significant changes during the initial charge, from the as-prepared high temperature γ_s ($P2_1/n$) phase to a more stable inverse β_{II} ($Pmn2_1$) polymorph [13]. As a consequence, all the Fe^{2+} and half the Li^+ share one set of tetrahedral sites with the remaining Li^+ occupying a second set of tetrahedral sites. Nytén et al. [14] have monitored the lithium extraction and insertion mechanism in Li_2FeSiO_4 by *in situ* XRD during the first two cycles. Only fully charged ($LiFeSiO_4$) and discharged states (Li_2FeSiO_4) were studied. Some *ex situ* XRD works have also revealed the structural change of Li_2FeSiO_4 during the initial charge and discharge [13,15].

In this study, a modified version of the cell design of Leriche et al. [4] was used for *in situ* XRD experiments, utilizing a conducting Kapton RS™ X-ray film as both the X-ray window and current collector in place of a Be window. Investigations by *in situ* XRD as well as EIS of a nanoporous Li_2FeSiO_4/C cathode was performed to study the structural and electrochemical property changes associated with the gradual change of composition x ($Li_{2-x}FeSiO_4$, $0 \leq x \leq 1$) and voltage during the initial cycle.

2. Experimental

2.1. Synthesis of nanoporous Li_2FeSiO_4/C

Nanoporous Li_2FeSiO_4/C was synthesized by a wet chemical method previously described [16]. A Li–Fe–Si-PVA solution (with the molar ratio Li:Fe:Si:PVA = 2:1:1:0.8) was prepared and stirred at 60 °C to form a gel, where $Li(CH_3COO)\cdot 2H_2O$ (Sigma–Aldrich, reagent grade), $Fe(NO_3)_3\cdot 9H_2O$ (Sigma–Aldrich, >98%), and tetraethyl orthosilicate (TEOS) (Aldrich, >99%) solutions were used as metal cation precursors. Polyvinylalcohol (PVA) (Aldrich, Mowiol 10–98, Mw = 61,000) was used as complexing and reducing agents during the carbothermal reaction. Gel formation took place after stirring for 6 h in an uncovered beaker. The gel was then covered and aged at 60 °C for 10 h before drying at 130 °C for 3 h. The Li–Fe–Si-containing dried gels were calcined at 450 °C for 1 h in air. The calcined powder was then mixed with an aqueous corn starch (Sigma–Aldrich, reagent grade) solution and ground into a paste in an agate mortar. The powder mixtures (starch content = 27 wt%) were heat treated in a flowing N_2 atmosphere at 650 °C for 10 h.

2.2. Characterization

The structural changes of the nanoporous Li_2FeSiO_4/C composite during the initial cycling were assessed using the *in situ* XRD electrochemical cell. Both a photograph and schematic drawing of the *in situ* XRD electrochemical cell setup are presented in Fig. S1. The cathode was prepared by mixing 90 wt% of the Li_2FeSiO_4/C composite with 8 wt% Supper-P carbon black, and 2 wt% polyvinylidene fluoride (PVDF) (Kynar, reagent grade) as a binder. A slurry was mixed by ball milling, using *N*-methyl-2-pyrrolidene (NMP) (Sigma–Aldrich, >99%) as the solvent. The electrodes were formed by tape casting the slurry onto the conductive surface of the Kapton, followed by drying overnight at 30 °C in a vacuum furnace. The *in situ* XRD electrochemical cell was assembled with the cathode, lithium metal as the anode and a Celgard 2400 film as the separator. The electrolyte used was 1 M $LiPF_6$ (Aldrich, ≥99.99%) dissolved in ethylene carbonate (EC, Sigma, 99%)/diethyl carbonate (DEC, Aldrich, ≥99%) (3:7 volume ratio). Cell assembly was carried out in an argon-filled glove box, where water and oxygen concentrations were 0.1 ppm. The cell was connected to a potentiostat (Voltalab 10) operating in chronocoulometric mode. The cell was charged/discharged instantaneously to 3000 mV, 3100 mV, 3200 mV, and 3250 mV/2500 mV and 1500 mV step by step and held till the charge current decreased to C/200 ($C = 160$ mA g^{-1}) in order to record the XRD patterns close to equilibrium. *In situ* XRD patterns were recorded with a Siemens D5000 diffractometer operating with a Cu Kα radiation (X-ray wavelength

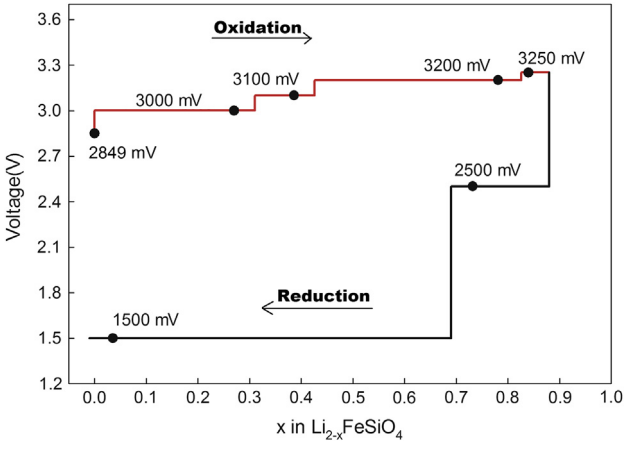

Fig. 1. Chronocoulometric profile for the initial charge and discharge of the nanoporous Li_2FeSiO_4/C cathode using the *in situ* XRD electrochemical cell. The red straight line is the oxidation (charge) profile and the black straight line is the reduction (discharge) profile. The black dots are the starting points for the XRD measurements. (For interpretation of the references to color in this figure legend, the reader is referred to the web version of this article.)

$\lambda = 0.15406$ nm). A graphite secondary monochromator was fitted into the diffractometer in order to reduce the fluorescence from Fe in the Li_2FeSiO_4 sample. Data were collected at 2θ from 15 to 48° with a step size of 0.02°, and 15 s per step (data collection time was 6.9 h per one potential step). Voltamaster 4 software was used to control the potentiostat and record the charge (Q) for every potential step. The composition x in $Li_{2-x}FeSiO_4$ can be calculated using Eq. (1):

$$x = \frac{\sum Q}{3.6 T_{cap} m} \quad (1)$$

where $\sum Q$ is the sum of the charge from the start point of applying electrical current and up to the start point of collecting XRD data. T_{cap} is the theoretical gravimetric capacity equal to 166 mAh g^{-1} for the Li_2FeSiO_4 system, and m is the mass of the cathode material, including the Li_2FeSiO_4 and secondary phases. In the initial state, the composition x is assumed to 0.

The electrochemical impedance spectra (EIS) of the nanoporous Li_2FeSiO_4/C composite during the initial cycling were assessed using a 3-electrode cell (Hohsen Corp.) with a metallic Li foil as reference and counter electrodes at 24 °C. The working electrode and electrolyte used were the same as the *in situ* XRD electrochemical cell. The 3-electrode cell was connected to a multichannel potentiostat (VMP-3, Princeton Applied Research) operating in galvanostatic intermittent titration technique (GITT) mode. The 3-electrode cell was charged or discharged for 1 h at a current density of C/16. A resting period of 5 h was imposed in order to record EIS close to equilibrium in the frequency range of 100 kHz–10 mHz. The ac amplitude was 5 mV peak-to-peak. The open-circuit potential was also recorded in order to obtain the coulometric titration curve (i.e. open-circuit voltage curve) [17]. The composition x in $Li_{2-x}FeSiO_4$ for each EIS data set was determined by the coulometric titration curve and the composition x is assumed to 0 in the initial state.

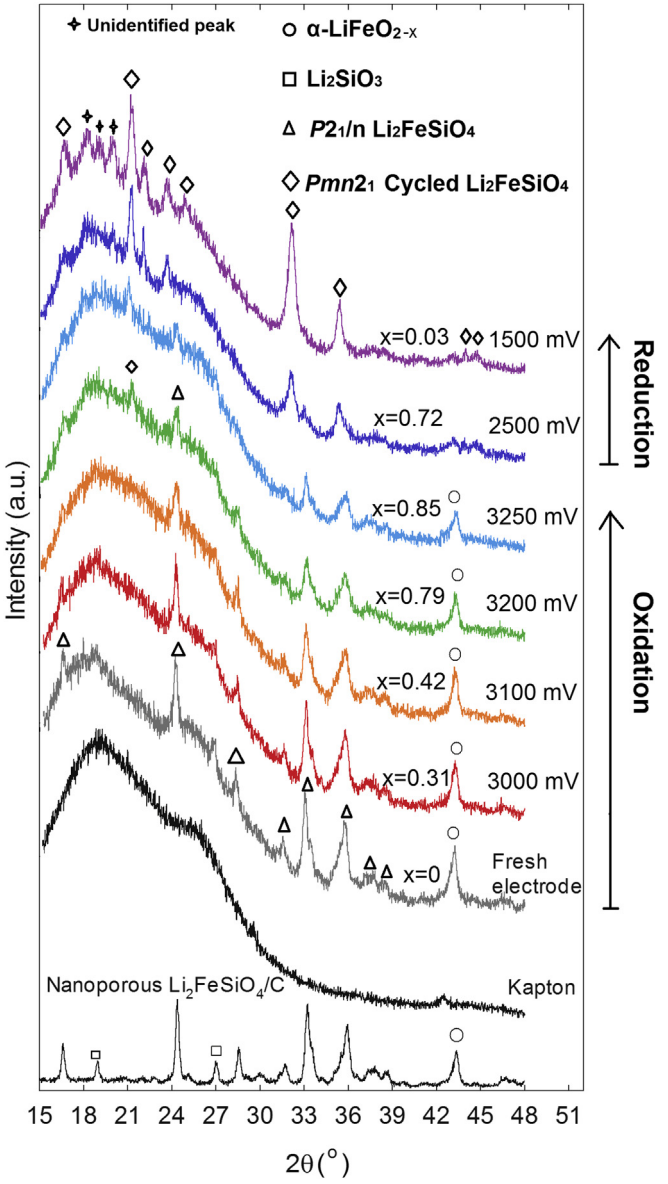

Fig. 2. *In situ* XRD patterns collected during the initial charge and discharge of the cell at different potential steps and composition x in $Li_{2-x}FeSiO_4$. XRD pattern of the nanoporous Li_2FeSiO_4/C powder. Diffractogram of Kapton and the fresh electrode are included in the bottom of the figure.

3. Results and discussion

Fig. 1 shows the chronocoulometry profile for the initial charge and discharge of the nanoporous Li_2FeSiO_4/C cathode using the *in situ* XRD electrochemical cell. The red line is the oxidation (charge) profile, and the black line is the reduction (discharge) profile, while the black dots are the starting points for the XRD measurements. It should be noted that during the XRD measurements, the composition x changed slightly, meaning the cell was not quite at equilibrium. However, this was considered insignificant for the purpose of these investigations.

Fig. 2 shows the *in situ* XRD patterns for different potential steps, where the composition x in $Li_{2-x}FeSiO_4$ at the starting point for each XRD measurement is listed next to the corresponding diffraction curve. The XRD patterns of the Kapton film and the initial nanoporous Li_2FeSiO_4/C powder are also included in Fig. 2,

Table 1
Summary of the observations in the *in situ* XRD patterns of the nanoporous Li_2FeSiO_4/C collected during the initial charge and discharge of the cell at different potential step. Composition x in $Li_{2-x}FeSiO_4$ is recorded at the start point for each XRD measurement.

Potential step (mV)	x (in $Li_{2-x}FeSiO_4$) at the starting point for collecting XRD data	Phase analysis			
		Li_2FeSiO_4 $P2_1/n$	Li_2FeSiO_4 $Pmn2_1$	α-$LiFeO_{2-x}$	Li_2SiO_3
Oxidation					
2849 (initial)	0	X		X	X
3000	0.31	X		X	X
3100	0.42	X		X	X
3200	0.79	x	x	X	X
3250	0.85	x	X	X	x
Reduction					
2500	0.72	x	X	x	x
1500	0.03		X	(x)	(x)

X: the font size of X expresses the relative amount of each phase indicated from the *in situ* XRD patterns.

(x): barely detectable from the XRD pattern

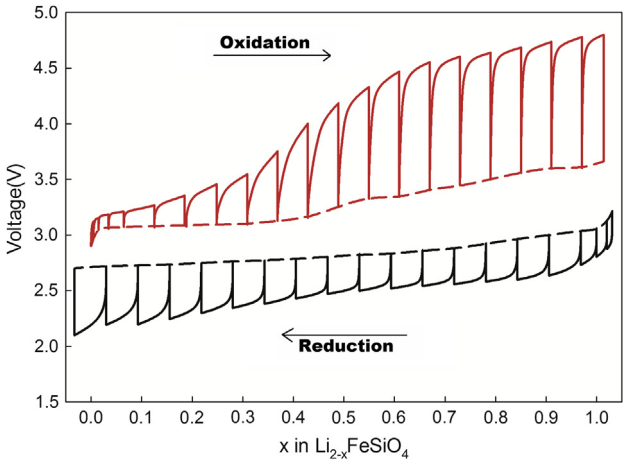

Fig. 3. Galvanostatic intermittent titration technique (GITT) profile for the initial charge and discharge of the nanoporous Li_2FeSiO_4/C cathode using a 3-electrode cell. The dashed lines are the corresponding coulometric titration curves derived from the GITT profiles.

where the Li_2FeSiO_4 phase could be identified by the space group $P2_1/n$ [18]. The additional diffraction line appearing at approximately 43° was ascribed to a α-$LiFeO_{2-x}$ related phase, while a Li_2SiO_3 secondary phase could also be observed in the pattern by the two diffraction lines appearing at 2θ values of approximately 19 and 27°. The XRD pattern of the Kapton film shows a broad feature in the low angle region, which naturally also appears in the XRD patterns of the electrode at different potentials. When the lithium extraction proceeded step by step from 3000 to 3250 mV, the intensity of the Bragg reflections from Li_2FeSiO_4 with space group $P2_1/n$ decreased and an additional peak at approximately 21° appeared at 3200 mV ($x = 0.79$). The intensity of this peak increased upon further Li^+ extraction from the crystal lattice at a potential of 3250 mV. Following the potential step at 3250 mV, the cell was discharged to 2500 mV before ending the discharge at 1500 mV. When 13 mol% Li^+ was re-intercalated into the lattice ($x = 0.72$), the diffraction lines corresponding to the $P2_1/n$ phase decreased significantly in intensity, while the peak at 21°, corresponding to the Li_2FeSiO_4 $Pmn2_1$ phase, still increased in intensity. In addition, new Bragg reflections appeared, which could also be ascribed to Li_2FeSiO_4 with space group $Pmn2_1$ [13]. At the same time, the peak at 43° from the α-$LiFeO_{2-x}$ related phase decreased in intensity. For the fully discharged cathode at 1500 mV, only the $Pmn2_1$ phase was observed. However, three unidentified peaks were found in the low Bragg diffraction angle region. It is not confirmed, but these might be due to a small change in symmetry of the $Pmn2_1$ phase. The above observations from the *in situ* XRD patterns, summarized in Table 1, suggest that a phase transformation of Li_2FeSiO_4 from $P2_1/n$ to $Pmn2_1$ occurred during the initial charge/discharge cycle, which is consistent with the analysis by Armstrong et al. [13]. The two phase coexistence in the XRD patterns suggests that the Li^+ de-intercalation follows a two phase process. During the discharge process, the $Pmn2_1$ phase forms continually and dominates in the fully discharged state. Interestingly, the amount of α-$LiFeO_{2-x}$ related phase is also reduced and is structurally changed during discharge. Kanno et al. [19] speculated that the conversion of a α-$LiFeO_2$ cathode material proceeds from the corrugated layer structure $LiFeO_2$ to an amorphous phase during the initial charge/discharge cycle, and further charge/discharge processes proceed in the amorphous phase. However, further studies are needed to verify this.

Fig. 3 shows the galvanostatic intermittent titration technique (GITT) profile for the initial charge and discharge of the nanoporous Li_2FeSiO_4/C cathode using the 3-electrode cell. The red and black solid lines are GITT profiles for the oxidation (charge) and the reduction (discharge), respectively, and the dashed lines are the corresponding coulometric titration curves derived from the GITT profiles. A plateau at a voltage of ~3.1 V can be seen in the oxidation coulometric titration curve, which can be attributed to the Fe^{2+}/Fe^{3+} redox potential [14]. And the plateau shifts to ~2.7 V in the coulometric titration curve for the reduction process. Large over-potentials are observed in the GITT profile, which imply that the electrode polarization was significant and the reaction was kinetically limited due to the low electronic and ionic conductivity of Li_2FeSiO_4 [20].

Fig. 4a and b presents the Nyquist plots of the nanoporous Li_2FeSiO_4/C sample measured during the initial charge/discharge cycle. All the plots consist of a small semicircle in the high-frequency

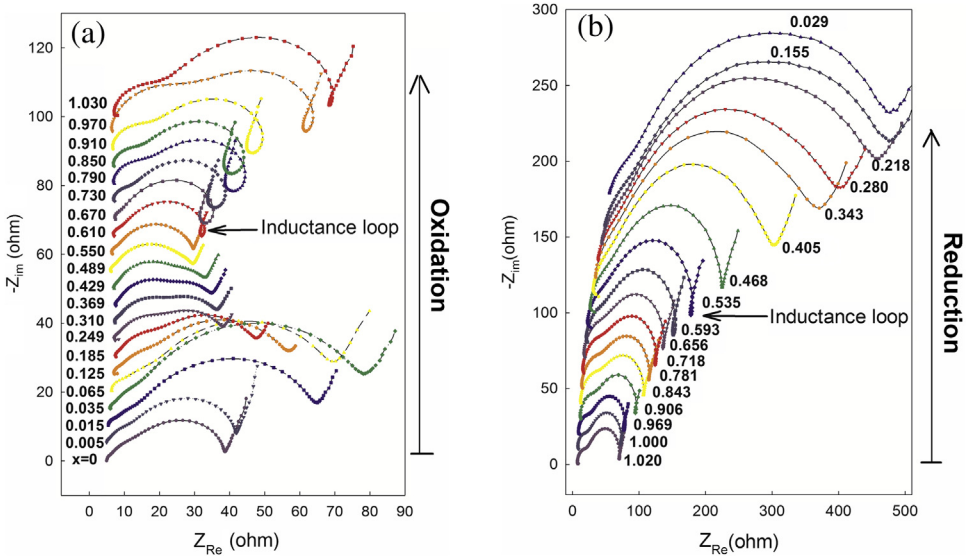

Fig. 4. Nyquist plots of the nanoporous Li_2FeSiO_4/C sample measured during the initial cycle at different composition x in $Li_{2-x}FeSiO_4$. (a) The oxidation (charge) process and (b) the reduction (discharge) process. The composition x in $Li_{2-x}FeSiO_4$ for each EIS data set was determined by the coulometric titration curve and the composition x is assumed to 0 in the initial state.

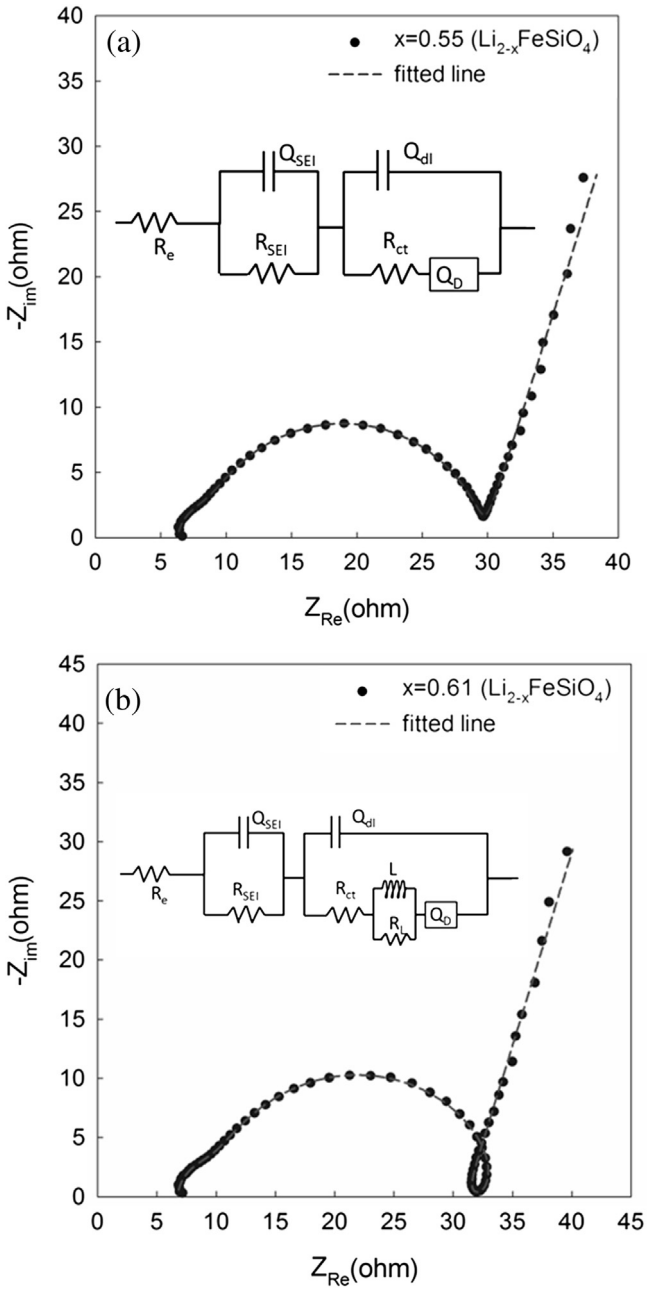

Fig. 5. Two different equivalent circuit models (a) with and (b) without inductance used to fit experimental impedance curves measured from nanoporous Li_2FeSiO_4/C electrode at a composition of $x = 0.55$ (a) and 0.61 (b) during the oxidation process.

region and a large semicircle in the high-to-medium frequency region, which are attributed to the lithium-ion migration through the SEI film and the charge-transfer through the electrode/electrolyte interface, respectively [21]. However, an important feature of the impedance spectra in the low frequency region is the appearance of an inductance loop starting at $x = 0.610$ during oxidation, and disappearing after $x = 0.535$ during reduction. These were only found during the initial cycle which is also where the two-phase region appeared, as indicated by *in situ* XRD (Fig. 2). A plausible explanation for the inductance loop is the formation of an electromotive force superimposed on the Li de-intercalation/intercalation. Most likely the inductance loop results from a concentration cell being established between the initial $P2_1/n$ Li-rich phase and the $Pmn2_1$ Li-poor phase of Li_2FeSiO_4 that appears during the first cycle. The Li^+ transport paths in the $Pmn2_1$ phase are quite different from those in the $P2_1/n$ phase, as revealed by Armstrong et al. [13], and involve distinct zigzag paths with a minimum Li migration barrier of 0.9 eV. In addition, the Li/Fe site-interchange in the $Pmn2_1$ phase opened alternative pathways, allowing three-dimensional percolation for Li-ion migration [14] which leads to more Li-ions being de-intercalated from the structure, forming a Li-poor region. Thus a concentration cell was established between the $P2_1/n$ Li-rich phase and the $Pmn2_1$ Li-poor phase separated by the phase boundary and a "leaky SEI film" [9]. A current flow within the concentration cell generated an electromotive force opposing the applied cell voltage. Such a situation meets the requirements for the formation of an inductance loop. During the discharge process, the concentration cell ($Li|P2_1/n||Pmn2_1|Li$) continued to leak current until the fully intercalated $Pmn2_1$ phase dominated, i.e. the Li^+ concentration differences in the electrode are removed, and the inductance loop disappeared as shown in Fig. 4b.

Based on the above analysis, two kinds of equivalent circuits were used to analyze the measured EIS data with and without inductance, as shown in Fig. 5a and b. These equivalent circuits based on the Voigt-type equivalent circuit analogs are widely used for simulation of electrodes for Li-ion batteries [22]. Here, R_e, R_{SEI}, and R_{ct} are resistances of the electrolyte, the SEI film, and the charge transfer reaction, respectively. The capacitance of the SEI film and the capacitance of the double layer are represented by the constant phase elements (CPE) Q_{SEI} and Q_{dl}, respectively, and account for the 'depressed semicircle' in the impedance spectra [23]. The phase transformation is simulated by an inductance L paralleled with a resistance of the phase boundary and leaky SEI film in the concentration cell (R_L). The low frequency region cannot be modeled properly by a Warburg diffusion element due to the phase transformation [24]. Therefore, the constant phase element (CPE), i.e. Q_D, was also used to replace the diffusion element [25]. This approach was used to obtain a good agreement between the calculated and the experimental data, which can be seen in Fig. 5a and b where the experimental and fitted impedance spectra corresponding to $x = 0.55$ (Fig. 5a) and 0.61 (Fig. 5b) during oxidation

Table 2
Values of the equivalent circuit parameters used for fitting the experimental curve.

Parameters	Description	Simulated parameters			
		$x = 0.55$	Uncertainty/%	$x = 0.61$	Uncertainty/%
R_e (Ohm)	Electrolyte resistance	6.3	0.5	6.7	0.5
R_{SEI} (Ohm)	SEI film resistance	1.9	7.2	2.7	6.4
Q_{SEI} (F)	Constant phase element of SEI film	9.9E-7	5.7	7.2E-7	4.7
R_{ct} (Ohm)	Charge transfer resistance	21.5	1	21.8	1.1
Q_{ct} (F)	Double layer capacitance	8.2E-6	8.2	7.7E-6	12.6
L (H)	Inductance	–		0.0024	10.6
R_L (Ohm)	Resistance of the phase boundary or leaky SEI film in the concentration cell	–		3.7	9

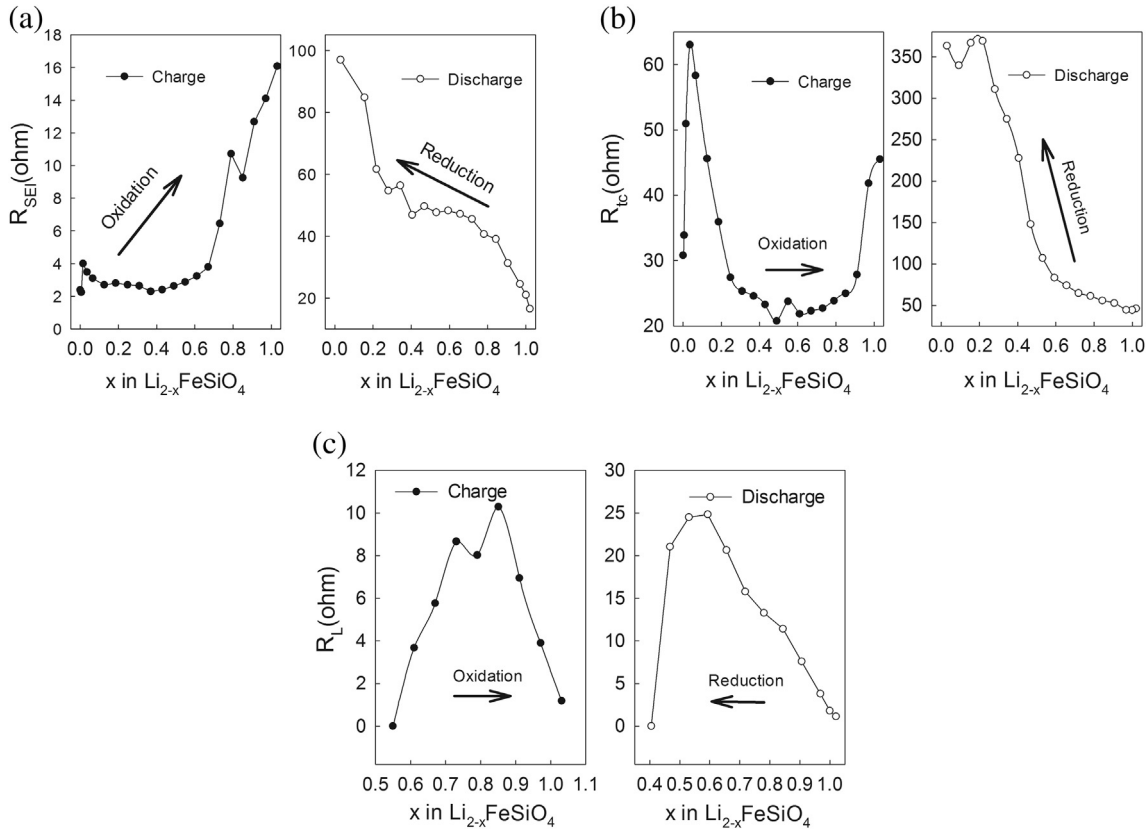

Fig. 6. Variations of (a) R_{SEI} (b) R_{ct} (c) R_L with composition x obtained from fitting the experimental impedance spectra of the nanoporous Li_2FeSiO_4/C electrode during the initial cycle.

are presented. The simulated electrochemical parameters are shown in Table 2.

Fig. 6a illustrates variations of R_{SEI} with composition x obtained from fitting the experimental impedance spectra of the nanoporous Li_2FeSiO_4/C electrode during the initial cycling. It can be seen that R_{SEI} stays almost constant below a composition of $x = 0.61$ in the initial charge process, indicating that the SEI film remained stable and unchanged to a certain extent in this process. However, R_{SEI} increased dramatically with the state of charge and voltage upon further oxidation, which might be due to an accelerated formation of the SEI film in the large over-potential region [26]. During discharge, R_{SEI} increased continuously which indicated a constant growth of the SEI film during the entire reduction process.

Fig. 6b shows the variations of R_{ct} with composition x during the initial cycle. It can be seen that R_{ct} reaches a minimum about half way through the oxidation process. R_{ct} is supposed to behave according to the following equation:

$$R_{ct} = \frac{RT}{nFi_0} \tag{2}$$

where F is the Faraday constant, R is the ideal gas constant, T is absolute temperature, and n is the number of electrons transferred per ion during the intercalation, which is 1 for Li^+. i_0 is the exchange current density, which can be express as Ref. [27]:

$$i_0 = nFc_{max}k_0(C_{Li^+})^{(1-\alpha)}(1-x)^{(1-\alpha)}x^{\alpha} \tag{3}$$

where c_{max} (mol cm^{-3}) is the maximum concentration of Li^+ in the insertion sites of the nanoporous Li_2FeSiO_4/C electrode, C_{Li^+} is the concentration of Li^+ in the electrolyte near the effective surface of the nanoporous electrode, and k_0 is the standard reaction rate constant, and α represents the symmetry factor for the electrochemical reaction and approximately equals to 0.5, supposing that the delithiation/lithiation process in the electrode is invertible [23]. Eqs. (2) and (3) clearly predict a rapid increase in R_{ct} as composition $x \rightarrow 1$ or $x \rightarrow 0$, i.e. in either completely intercalated or de-intercalated state, and a minimum for a composition of $x = 0.5$. The experimental data therefore corresponds reasonably well with the values predicted according to these equations.

Fig. 6c shows the variations of R_L with composition x during the initial cycle. A maximum can be found at a composition of $x = 0.85$ in the charge process, indicating large amounts of phase boundaries, leaky SEI films and large differences in the Li^+ concentration in the electrode resulting from the phase transformation. This coincides well with the *in situ* XRD results which show the coexistence of the two phases at a composition of $x = 0.85$ (Fig. 2). During the discharge process, R_L increases to reach a maximum at approximately $x = 0.6$ whereupon it continues to decrease to zero for $x = 0.4$. This initial increase in R_L during the reduction process may be due to the increased differences in the Li^+ concentration distribution when the Li^+ is re-intercalated into the electrode. The reduction of R_L to zero after further discharge indicates that the $Pmn2_1$ phase dominates the fully intercalated electrode, which is consistent with the XRD results.

4. Conclusions

An *in situ* X-ray diffraction electrochemical cell was fabricated with an electrically conductive Kapton polyimide film used as both the X-ray window and current collector. Using this *in situ* cell, a phase transformation of the nanoporous Li_2FeSiO_4/C cathode material was detected. The coexistence of a $P2_1/n$ phase and a $Pmn2_1$

phase in the *in situ* XRD patterns was first observed at 3200 mV, corresponding to a composition of $x = 0.79$ in $Li_{2-x}FeSiO_4$. This suggests that the Li^+ de-intercalation follows a two phase process. The XRD data showed that the $Pmn2_1$ phase dominated in the fully discharge state, which was confirmed by the presence of an inductance loop in the low frequency region of the electrochemical impedance spectra. We attribute the inductance loop to the formation of a ($Li|P2_1/n||Pmn2_1|Li$) concentration cell from which current flows in opposition to the Li being intercalated into the electrode. The current flow occurs in the ($Li|P2_1/n||Pmn2_1|Li$) concentration cell due to the $P2_1/n$ Li-rich phase and the $Pmn2_1$ Li-poor phase being separated by a phase boundary and a leaky SEI film. Once the cell has completed the first charge/discharge cycle and the $Pmn2_1$ phase has been formed the inductance loop does not appear in the impedance spectra. Two different equivalent circuit models, with and without inductance, have been proposed, which fit the experimental data well. This combination of *in situ* XRD with EIS of the nanoporous Li_2FeSiO_4/C cathode material, gives a clearer view of the phase transformation of Li_2FeSiO_4 during the initial charge/discharge cycle.

Acknowledgments

The authors would like to thank DuPont for providing us with the Kapton RS films and Dr. Julian R. Tolchard (Department of Material Science and Engineering, NTNU) for help with the design of the modified *in situ* XRD cell.

Appendix A. Supplementary data

Supplementary data related to this article can be found at http://dx.doi.org/10.1016/j.jpowsour.2013.03.193.

References

[1] P. Poizot, S. Laruelle, S. Grugeon, L. Dupont, J.M. Tarascon, Nature 407 (2000) 496–499.
[2] R.R. Chianelli, J.C. Scanlon, B.M.L. Rao, J. Electrochem. Soc. 125 (1978) 1563–1566.
[3] J.R. Dahn, M.A. Py, R.R. Haering, Can. J. Phys. 60 (1982) 307–313.
[4] J.B. Leriche, S. Hamelet, J. Shu, M. Morcrette, C. Masquelier, G. Ouvrard, M. Zerrouki, P. Soudan, S. Belin, E. Elkaïm, F. Baudelet, J. Electrochem. Soc. 157 (2010) A606–A610.
[5] E.A. Meulenkamp, J. Electrochem. Soc. 145 (1998) 2759–2762.
[6] Dupont, DuPont™; Kapton® RS Data Sheet (2008).
[7] E. Rabkin, V.M. Skripnyuk, Scr. Mater. 49 (2003) 477–483.
[8] J. Hong, C. Wang, U. Kasavajjula, J. Power Sources 162 (2006) 1289–1296.
[9] J.S. Gnanaraj, R.W. Thompson, S.N. Iaconatti, J.F. DiCarlo, K.M. Abraham, Electrochem. Solid-State Lett. 8 (2005) A128–A132.
[10] M. Itagaki, N. Kobari, S. Yotsuda, K. Watanabe, S. Kinoshita, M. Ue, J. Power Sources 148 (2005) 78–84.
[11] Q. Zhuang, X. Fan, J. Xu, G. Wei, Q. Dong, S. Sun, Chem. Res. Chin. Univ. 24 (2008) 511–515.
[12] D. Lv, W. Wen, X. Huang, J. Bai, J. Mi, S. Wu, Y. Yang, J. Mater. Chem. 21 (2011) 9506–9512.
[13] A.R. Armstrong, N. Kuganathan, M.S. Islam, P.G. Bruce, J. Am. Chem. Soc. 133 (2011) 13031–13035.
[14] A. Nytén, S. Kamali, L. Haeggstroem, T. Gustafsson, J.O. Thomas, J. Mater. Chem. 16 (2006) 2266–2272.
[15] A. Kojima, T. Kojima, T. Sakai, J. Electrochem. Soc. 159 (2012) A525–A531.
[16] H. Zhou, M.-A. Einarsrud, F. Vullum-Bruer, Solid State Ionics 225 (2012) 585–589.
[17] S.-W. Kim, S.-I. Pyun, Electrochim. Acta 46 (2001) 987–997.
[18] A. Boulineau, C. Sirisopanaporn, R. Dominko, A.R. Armstrong, P.G. Bruce, C. Masquelier, Dalton Trans. 39 (2010) 6310–6316.
[19] R. Kanno, T. Shirane, Y. Inaba, Y. Kawamoto, J. Power Sources 68 (1997) 145–152.
[20] R. Dominko, D.E. Conte, D. Hanzel, M. Gaberscek, J. Jamnik, J. Power Sources 178 (2008) 842–847.
[21] Q. Zhuang, T. Wei, L. Du, Y. Cui, L. Fang, S. Sun, J. Phys. Chem. C 114 (2010) 8614–8621.
[22] M.E. Orazem, P. Agarwal, L.H. Garcia-Rubio, J. Electroanal. Chem. 378 (1994) 51–62.
[23] M. Holzapfel, A. Martinent, F. Alloin, B. Le Gorrec, R. Yazami, C. Montella, J. Electroanal. Chem. 546 (2003) 41–50.
[24] X. Fan, Q. Zhuang, G. Wei, L. Huang, Q. Dong, S. Sun, J. Appl. Electrochem. 39 (2009) 1323–1330.
[25] T. Piao, S.M. Park, C.H. Doh, S.I. Moon, J. Electrochem. Soc. 146 (1999) 2794–2798.
[26] D. Ensling, M. Stjerndahl, A. Nytén, T. Gustafsson, J.O. Thomas, J. Mater. Chem. 19 (2009) 82–88.
[27] S. Xu, Q. Zhuang, L. Tian, Y. Qin, L. Fang, S. Sun, J. Phys. Chem. C 115 (2011) 9210–9219.